Shock Induced Reaction Observed via Ultrafast Infrared Absorption in Poly(vinyl nitrate) Films

S. D. McGrane,* D. S. Moore, and D. J. Funk

Dynamic Experimentation Division, DX-2, Los Alamos National Laboratory, MS P952, Los Alamos, New Mexico 87545

Received: April 7, 2004; In Final Form: August 12, 2004

Ultrafast laser shock generation methods and broad-band infrared reflection absorption spectroscopy have provided evidence that shock-induced chemistry in a condensed-phase energetic material occurs on a time scale of tens of picoseconds and involves the nitro group as a primary reactant. Femtosecond broad-band infrared reflection absorption spectroscopy was used to monitor films of the energetic polymer poly(vinyl nitrate) during shock loading and rarefaction. At ∼18 GPa, poly(vinyl nitrate) films exhibited loss of absorption in the nitro group stretch modes that did not recover upon rarefaction, providing an indication of initial chemical reaction. At pressures ≤9 GPa, the observed spectral changes are ascribed to thin film optical interference effects, without chemical reaction. The loss of infrared absorption required an induction time of tens of picoseconds after shock passage, supporting reaction mechanisms that require vibrational energy transfer rather than prompt reaction.

1. Introduction

Observation of shock induced chemistry offers insight into the molecular scale response[1−10] to extreme conditions of temperature and pressure, and is required to construct a comprehensive understanding of detonation.[11] The physics of detonation has strong theoretical and experimental foundations,[12] yet very few studies shed light on the chemistry occurring following the passage of a shock wave. Large scale shock experiments are unable to resolve either the time and length scales or the detailed reaction pathways that are important for validation of molecular level simulations of physical[13−15] and chemical[16−18] shock processes, while small scale studies do not reach steady detonation and may miss mesoscopic effects such as interface boundaries. Thus, small scale studies complement gas guns in achieving a more complete understanding of shock physics and chemistry. Small scale studies are also sensitive to the initial events that occur upon shock loading, which are crucial in determining the sensitivity of the material toward accidental detonation. Prediction of initiation requires a framework that includes a mechanism for the shock wave energy to couple into molecular bonds. While various theories have been proposed regarding the shock induced reaction mechanism, there are few experiments sensitive to the time and length scales involved in testing them, or in observing the subsequent chemical kinetics.

Traditional gas gun experiments have formed the foundations for shock physics, but spectroscopic monitoring of chemical details in bulk (millimeter to centimeter) shocked samples at nanosecond time scales is very difficult due to both shock induced sample opacity (due to the sample thickness) and potentially subnanosecond reaction rates. We have developed methods that can generate[19] and characterize[20−23] similar shocks on very small scales—submicron thicknesses with subpicosecond time resolution—specifically to enable spectroscopic monitoring of shock induced chemistry.

In this article, we show the first observations of shock induced reaction that use microscopic shocks and femtosecond diagnostics to access scales amenable to molecular dynamics scale simulations. At ∼18 GPa, poly(vinyl nitrate) (PVN) films exhibited loss of nitro stretch absorptions that did not recover upon rarefaction, indicating chemical reaction. At ≤9 GPa, observed spectral changes are ascribed to optical interference effects, without chemical reaction. The loss of infrared absorption required an induction time of tens of picoseconds after shock passage, supporting reaction mechanisms involving vibrational energy transfer over prompt reaction.

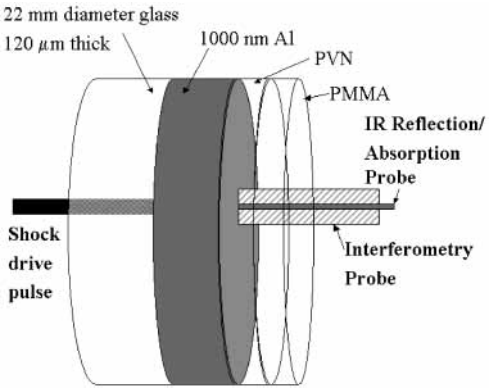

Figure 1. Experimental geometry. Shock drive pulse is ∼250 ps temporally shaped,[19] 0.6−6 mJ, incident at 0° through the glass onto the Al with a 80 μm spot size (Gaussian fwhm). Infrared probe pulse is ∼170 fs, centered at λ = 6150 or 7880 nm (1270 or 1625 cm^{-1}, with a spectral bandwidth of >130 cm^{-1}), incident at 11° with a 45 μm spot size. Interferometry probe is ∼170 fs at λ = 800 nm with a spot size > 500 μm fwhm. Poly(methyl methacrylate) (PMMA) layer is present only on "double stack" experiment reported in Figure 5, while the poly(vinyl nitrate) (PVN) layer is present in all the experiments.

2. Experimental Section

2.1. Experimental Geometry. The arrangement of pump, probes, and thin films in the experimental geometry is illustrated in Figure 1. The shock drive, or pump, pulse travels through

10.1021/jp048464x CCC: $27.50
Published on Web 09/28/2004

the glass substrate and is partially absorbed at the glass/aluminum (Al) interface. This generates a plasma that continues to absorb the pump pulse, and the confined expansion of the plasma drives a shock into the Al. This shock is transferred into the PVN thin film when it reaches the Al/PVN interface. The second polymer film, poly(methyl methacrylate) (PMMA), is present only for the "double stack" experiment shown in Figure 5. The polymer films are mechanically pumped by the shock, while the Al protects them from being directly affected by the shock drive laser pulse. The sample is rastered to provide a fresh shocked region between shots, providing several hundred to thousands of shots on a 22 mm diameter substrate.

2.2. Laser Shocks and Ultrafast Interferometric Microscopy. The shock generation method,[19] ultrafast interferometric microscopy,[20] and techniques for measurement of shock velocity, particle velocity, and shocked refractive index[21,22] have been presented in detail elsewhere. Briefly, a 10 Hz, 50 mJ, 120 fs Ti:sapphire chirped pulse amplified laser system (Spectra Physics TSA 50) is used to generate a chirped, spectrally chopped pulse to drive the shock with a ~10 ps rise and ~200 ps of nearly constant pressure. The remainder of the pulse is compressed to <170 fs (deconvolved from single shot autocorrelation assuming a sech^2 pulse profile in time) and used to perform interferometric microscopy and to pump an optical parametric amplifier (OPA) to generate broad-band mid-infrared pulses. The pump pulse time delay is scanned relative to the interferometric and mid-infrared probes to build the time history, and the sample rastered between shots. The reproducibility of the shocks and the uniformity of the thin films allow several shots (typically 3−10) to be averaged for each time point; the shot spacing of ≤600 μm and the finite sample size provide practical upper limits on the number of shots averaged.

The ultrafast interferometric microscopy technique[20] provides spatially and temporally resolved snapshots of the changes in phase and reflectivity at every shock (at ~0.5 Hz). The interferometry probe pulse is >500 μm full width at half-maximum (fwhm), encompassing the shocked region and some unshocked material. The reflection from the sample surface is imaged onto a CCD, providing spatial resolution of ~2 μm in the directions transverse to the shock. Sensitivity to phase changes caused by surface motion is subnanometer in the shocked direction. Temporal resolution is governed by probe pulse width and angle of incidence.

The changes in phase are due to both motion of the shocked material and changes in refractive index.[20−22] Refractive index changes are particularly useful for the shocked polymers, where oscillations in the phase change versus time provide a means of tracking where the shock front is in the material. This requires fitting of phase shift versus time and is far more sensitive if data are taken at multiple angles, particularly near-normal and glancing angles, both at two orthogonal polarizations. These multiple angle/multiple polarization data are simultaneously fit to thin film equations to determine the shock velocity, particle velocity, and shocked refractive index. This method was used to derive Hugoniot information on the laser shocked PVN and PMMA thin film samples.[21−22]

The interferometry is extremely sensitive to any perturbation in position or refractive index. Small refractive index changes in the Al[23] (≤0.1 rad) can be seen for the first several picoseconds until the surface motion quickly makes them negligible. At the highest shock strengths, a much weaker laser prepulse (~10^{-3} of the pump energy) contributes up to 0.2 rad phase shift, which is subtracted out. The spatial and temporal reflectivity (at 800 nm) maps are also determined simultaneously, but have not been analyzed in detail for the work reported here.

2.3. Mid-Infrared Generation and Application. The OPA (Spectra Physics OPA 800) was used to generate tunable signal and idler pulses that were then focused near a difference frequency generation (DFG) crystal ($AgGaS_2$) to generate tunable mid-infrared with a frequency bandwidth of >130 cm^{-1} fwhm. The DFG was performed close to the sample, ~0.5 m, to avoid absorption lines from atmospheric water broadening the pulse appreciably. The signal and idler were removed with a pair of dielectric long pass filters with cut-on wavelengths at 2.5 and 5 μm. The interferometry probe (800 nm) and mid-IR probe (5−9 μm) were overlapped in time by monitoring the mid-IR transmission of a 250 μm thick Si wafer in the target position as a function of relative delay. The cross correlation derived in this manner was used to set the relative interferometry probe/mid-IR probe delays to within 1 ps. Size and spatial overlap of the mid-IR pulse with the pump pulse was monitored by measuring the change in reflection for various size holes generated by shocking Al films, and by transmission through pinholes.

The infrared pulse traversed a metallic beam splitter (approximately equal transmission/reflection) to form a reference pulse and a pulse that was focused on the sample (spot size ~45 μm diameter fwhm) with a 2 in. focal length BaF_2 lens. The mid-IR was transmitted through the thin polymer film, reflected off the Al film, and transmitted through the polymer film again before being collimated with a 3 in. focal length BaF_2 lens. Both the sample and reference mid-IR pulses were then imaged collinearly through a monochromator (Oriel 0.125 m, 75 g/mm grating blazed at 7 μm, 120 μm entrance slit) but displaced vertically to produce two stripes on a liquid nitrogen cooled 256 × 256 pixel HgCdTe focal plane array (SE-IR, Indigo chip). Differences in collection efficiency between sample and reference arm were corrected by placing an Al mirror (identical to the Al mirror on which the samples were deposited) at the target position. Referencing the sample to the reference stripe allowed single shot spectra to be taken with a typical accuracy of <5% (transmission units) across a 150−200 cm^{-1} range. Pulse-to-pulse variability of the mid-IR could not be improved with the 10 Hz Ti:sapphire amplifier pump lasers (532 nm Quanta Ray GCR-170 and PRO-190) employed, and the infrared intensity and spectral fluctuations are the primary noise source in the experimental data. Limited preliminary IR absorption data were presented in ref 24.

Wavelength calibration of the infrared spectra was performed with weak water line absorptions (occurring primarily between the sample and the detector) in the reference and sample spectra in the range 1500−1750 cm^{-1}. Calibration in the range 1150−1350 cm^{-1} began by using the peak absorption from the Fourier transform infrared (FTIR) spectrum to provide the absolute wavenumber at the peak. Determining the wavenumber width per pixel involved scanning the center wavelength to move the peak absorption to the edges of the image and reading the monochromator setting (backlash compensated), which agreed well with the water line calibration in the 1500−1750 cm^{-1} range. The pixel sizes at the magnifications employed in each series of experiments were 0.72 and 1.24 cm^{-1} for the ranges 1150−1350 and1500−1750 cm^{-1}, respectively. Resolution with the 120 μm slit width is approximately 13 nm or 2.0 and 3.4 cm^{-1} at the central wavenumbers 1270 and 1630 cm^{-1}, respectively.

2.4. Pressure. The infrared spot size was approximately 45 μm fwhm, whereas the shock pump has a Gaussian profile with

fwhm of 80 μm. This size ratio leads to a distribution of pressures observed by the infrared probe. The pressures given in the results are determined by the interferometric measurements of the shock and particle velocity spatially averaged over the central 30 μm diameter of the shock. The pulse energy to pressure mapping in PVN under the conditions noted above was 6.0, 3.0, 1.6, 0.6 mJ → 18, 17, 9, 7 GPa.[22,25] Pressures determined in this manner are approximately equal to the most likely (statistically) pressure sampled by the probe, but the average pressures are somewhat lower (factor 0.8) due to the tail of infrared spatial intensity into regions of low pump pulse intensity.

Note that multiple angle, multiple polarization interferometry, or dynamic ellipsometry, allows determination of the shock velocity (u_s), particle velocity (u_p), and shocked refractive index, but the unshocked density (ρ_0) must also be known to determine the shock pressure (P_s) via the shock jump equation $P_s - P_0 = \rho_0 u_s u_p$.[11] Measurement of the dynamic ellipsometry for the PVN films, as a function of pump energy, determined each u_s and u_p pair with ~5% precision. The change in refractive index (at 800 nm) was also determined, but was not needed for the results reported in this paper. The full density ($\rho_0 = 1.186$ g/cm^3) is used for PMMA, justified by measurement of the full refractive index at 632.8 nm ($n = 1.49$) of our spin-coated thin films to within $\Delta n = 0.02$. The density of the bulk PVN measured by gas pychnometry is $\rho_0 = 1.34$ g/cm^3. The bulk material refractive index measured with index matching fluids is $n = 1.508 \pm 0.003$ (average value for white light). The value we determine for our spin-cast films at 632.8 nm is $n = 1.50 \pm 0.03$, indistinguishable from the bulk value. The value $n = 1.50$ was used as the unshocked value for 800 nm interferometry, since we are far from any absorption resonances at both 632.8 and 800 nm. An uncertainty in n of ± 0.03 translates into a density uncertainty of 5% via the Lorentz−Lorenz equation, essentially $\rho \propto (n^2 - 1)/(n^2 + 2)$. Although the samples are likely to be full density, up to 5% porosity may be present (note that pores would have to be submicron due to submicron film thickness and to avoid observation via the interferometric microscopy performed on the samples). Assuming all errors are additive in quadrature provides pressure uncertainties of 10%.

2.5. Thin Film Preparation and Characterization. The polymer thin films were spin-coated onto 1 μm Al films, which had been vapor deposited onto 120 μm thick, 22 mm diameter BK-7 glass substrates. The solvents and spin-coating conditions used to prepare the thin films as well as the characterization methods have been described in detail elsewhere.[21] The PVN (molecular structure $(-CH(-ONO_2)CH_2-)_n$) used was 14.5% N by mass, molecular weight 77 000−79 000. Film thicknesses were measured with white light spectral reflectivity (Filmetrics) and were uniform to within typically 2% across the region of the sample used in the experiments. The PVN/PMMA films were formed by spin coating PVN onto the Al from *n*-butyl acetate, measuring the thickness, and then spin coating the PMMA from toluene solvent. The combined thickness agreed with the thickness from spinning the two films on different substrates and adding the total thickness; there were no signs of dissolution of the PVN film when spin coating the PMMA film (using a different solvent).

2.6. Static Complex Refractive Index Measurement. The complex refractive index of PVN was determined by infrared spectral ellipsometry. The FTIR spectrum was acquired with a Bruker Equinox 55 with XA 511 air−water interface attachment for five thicknesses at 12 angles and two polarizations. These 120 spectra were simultaneously fit to the thin film equations for the two unknowns, the real and imaginary parts of the refractive index, versus wavenumber as detailed in ref 27, employing the Kramers−Kronig relations over the entire spectral range to improve the convergence of the fitting procedure.

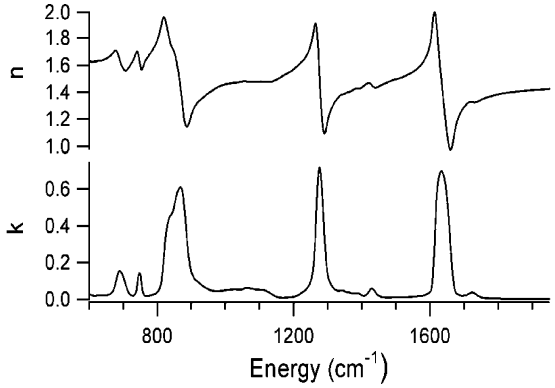

Figure 2. Complex refractive index of PVN. Real (n) and imaginary (k) parts of the PVN infrared refractive index determined by spectral ellipsometry, used to account for thin film interference in the spectral calculations.

3. Results

3.1. Static Complex Refractive Index of PVN. Analysis of the infrared spectra requires accounting for thin film interference effects, which, upon shock compression, change the composite reflectivity. To analyze the thin film interference effects, the infrared complex refractive index spectra for ambient samples of PVN (molecular structure $(-CH(-ONO_2)CH_2-)_n$) and the inert poly(methyl methacrylate) (PMMA)[27] were determined. This was accomplished by recording FTIR spectra at 12 angles and two orthogonal polarizations for five film thicknesses, followed by fitting the data to the thin film equations. The real and imaginary parts of the PVN refractive index are shown in Figure 2; the PMMA results were presented in ref 27.

3.2. Broad-Band Infrared Absorption in Shocked PVN. *3.2.1. Simulations of Shocked Thin Film Spectra.* Simulations of the infrared absorption spectra during shock loading were performed to help isolate the spectral changes that originate in chemical reaction, temperature, or pressure effects, from those that originate in dynamic thin film interference effects. The shocked spectral simulations used the measured static complex refractive index, along with the assumption that the imaginary part of the refractive index increased proportionally to the density increase upon shock compression. This assumption is similar to the Gladstone−Dale type model of the shocked refractive index, but near an absorption resonance the imaginary part must scale with the real part due to Kramers−Kronig relations.[27] The assumption is essentially equivalent to neglecting any chemical change, pressure, or temperature shifts, including only the effect of higher density after uniaxial compression or keeping the individual molecular cross sections constant. While this does not capture the true dynamics, it provides a baseline; the differences between this baseline and the experimental data enable the true spectral changes to be isolated from the prominent thin film interference effects.

The real part of the shocked refractive index was determined by a Kramers−Kronig transform of the scaled imaginary part in the range 600−2000 cm^{-1}. This procedure and the refractive index spectrum of PMMA are detailed in ref 27. The shock and particle velocity, and the shocked density change, were determined with multiple angle and polarization interferometry as reported in refs 21 and 22. The rarefaction wave is also

modeled here, for comparison with the late time experimental data. When the shock reaches the air interface, a rarefaction wave is propagated back into the compressed material, taking the material back to its original density at zero pressure. The rarefaction was divided into 1 GPa pressure steps that propagate back into the compressed material with a pressure-dependent velocity approximated using eq 1, where c is the sound speed and c_0 and s are the intercept and slope of the experimental plot of the Hugoniot (shock velocity u_s versus particle velocity u_p) in the range studied (7−18 GPa). Equation 1 approximates the unloading isentrope with the reflected Hugoniot. A given pressure P has a corresponding u_s and u_p which then determines $c(P)$.[28]

$$c = \frac{(c_0 + 2su_p)(c_0 + (s-1)u_p)}{c_0 + su_p} \qquad (1)$$

$$u_s = c_0 + su_p$$

In this manner the dispersion of the rarefaction is approximated. Shock impedance matching[11,28] between PVN and PMMA was used to find the initial partial rarefaction of the PVN, from 18 to 17 GPa, in the PVN/PMMA double stack experiment (accounted for in the spectral calculations of Figure 5). No pressure or temperature shifting, or chemical reaction, was incorporated into the spectral simulation model because the effect of the shock wave on the vibrational spectrum cannot be predicted without extensive further modeling of these shocked molecular systems. The deviation of the experimental data from our spectral simulations indicate pressure, temperature, and reaction effects that are precisely the focus of this work.

3.2.2. PVN Symmetric Nitro Group Stretch. The effects of shock loading on the infrared absorption resonance (measured in reflectance) associated with the 1270 cm^{-1} symmetric nitro group stretch,[29] $\nu_s(NO_2)$, of 940 nm thick PVN films (thickness uncertainties ∼2%) are shown as a function of shock pressure in Figure 3. The spectral data are distributed on the x-axis, and the y-axis defines the time since the shock wave has entered the polymer film, determined interferometrically. The calculated spectra[27] include only thin film effects and do not account for pressure and temperature shifts or chemical reaction. The areas of disagreement between the calculated and observed shocked spectra are thus the areas of most interest. In Figure 3, spectra at 7 and 9 GPa exhibit loss of absorption followed by substantial recovery, as expected for thin film interference. In contrast, data at 17 and 18 GPa show a permanent loss of absorption, as expected for chemical reaction. Note that the low-pressure shocks travel more slowly, so the time scales for shock and rarefaction are longer than at higher pressures. The 9 GPa peak reflectance increases from 0.14 to 0.73, and then recovers to 0.20 as the rarefaction wave releases the sample pressure. In contrast, when the sample is shocked to 17 GPa, the reflectance changes to 0.79, and then recovers only slightly to 0.71. The 7 and 9 GPa data show more reflectance than the fully shocked calculated spectra, which we tentatively attribute to temperature and pressure effects on the index of refraction that are unaccounted for in the calculation. Full interferometric analysis of the pressure profile and rarefaction at times over 200 ps, where the 7 and 9 GPa infrared absorption recovery is seen, is currently underway. However, recovery of the reflectance upon rarefaction (at 7 and 9 GPa) indicates that the origin of the spectral changes is predominantly thin film interference, whereas lack of recovery upon rarefaction (at 17 and 18 GPa) is indicative of chemical reaction.

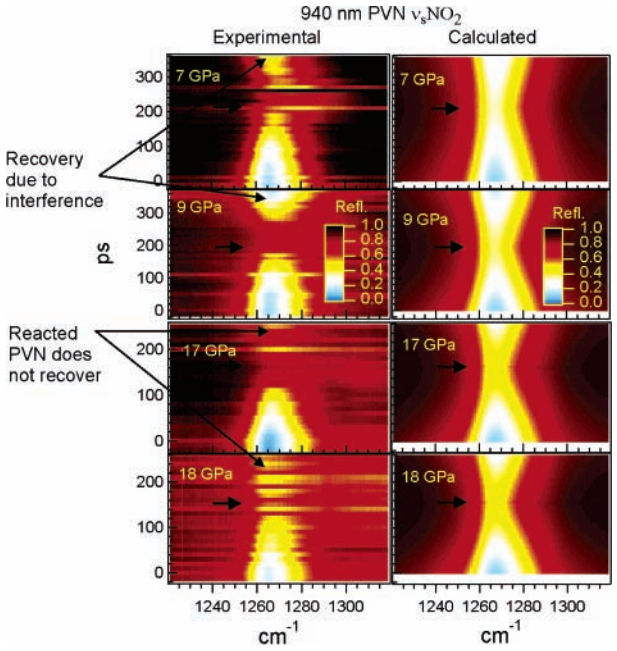

Figure 3. Time-resolved infrared absorption (in reflectance units) in the $\nu_s(NO_2)$ spectral region of 940 nm thick PVN shocked between 7 and 18 GPa. Calculated plots include only thin film interference, excluding pressure and temperature shifts and chemical reaction, making the differences between the experimental and calculated spectra the primary subjects of interest. Shock pressures were determined by interferometry.[22] Arrows show the time at which the shock has fully traversed the film and rarefaction begins.

3.2.3. PVN Antisymmetric Nitro Group Stretch. The effects of shock loading on the 1625 cm^{-1} antisymmetric nitro group stretch band, $\nu_{as}(NO_2)$, of 940 nm PVN films are shown in Figure 4A. The increase in reflectance at the $\nu_{as}(NO_2)$ resonance is less complete, when fully shocked, than observed in the symmetric stretch. In all cases, the fully shocked PVN exhibits greater increases in reflectance than the thin film interference calculations predict, and the loss of absorption persists into the rarefaction. To more clearly understand the $\nu_{as}(NO_2)$ mode behavior, especially during the rarefaction, we repeated the 18 GPa experiment with a 700 nm PVN film; the infrared absorption spectra are shown in Figure 4B. The loss of the 700 nm PVN $\nu_{as}(NO_2)$ absorption is far more obvious, and clearly does not recover during rarefaction. The differences seen in Figure 4 illustrate that changing film thickness affects the thin film interference effects, and other potential interfering factors that are not yet understood including the time available for reaction, product buildup, subsequent reactions, and potentially the change of shock strength at long times.

3.2.4. Shocked PVN/PMMA Double Layer. The above evidence for chemical reaction, i.e., loss of $\nu_{as}(NO_2)$ and $\nu_s(NO_2)$ mode absorption strength, occurred partly at times when the rarefaction is traversing back through the shocked sample, especially obvious in Figure 4B. This fact raised the possibility that the rarefaction plays an essential role in the loss of absorption. To address this possibility, a multilayer film experiment was performed.

A 440 nm window of inert PMMA was spin-coated onto 575 nm of PVN. The PMMA layer maintains the pressure in the PVN after the shock wave has passed. Figure 5 shows the time-dependent IR absorption spectra (measured in reflectance) in the $\nu_{as}(NO_2)$ mode region during shock and rarefaction. The shock or rarefaction reaches various interfaces at the arrows t_0−t_4, as denoted in the caption (using shock and particle velocities from refs 21 and 22, uncertainties ∼5%). Since the

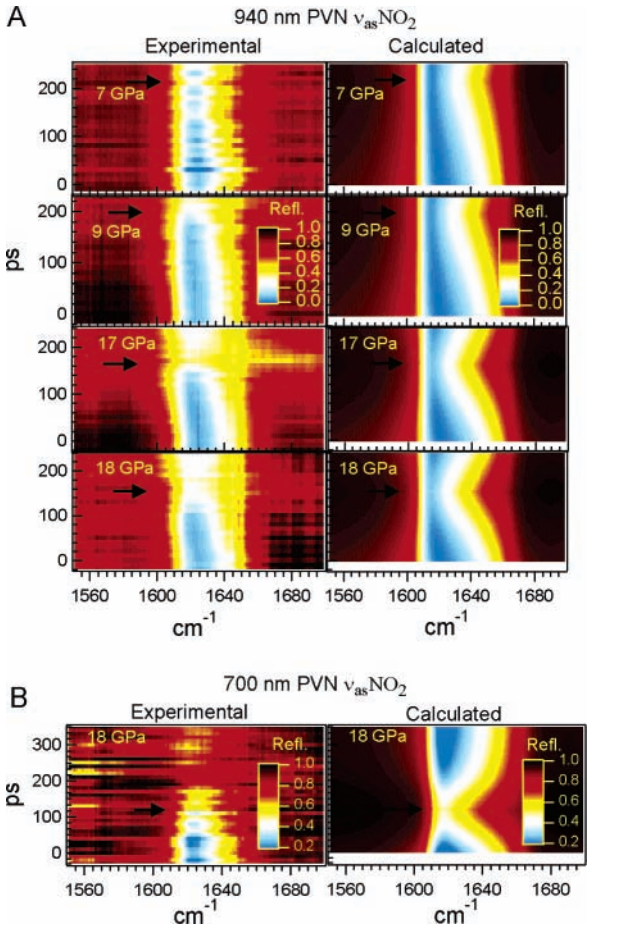

Figure 4. Time-resolved infrared absorption (in reflectance units) in the $\nu_{as}(NO_2)$ spectral region of (A) 940 nm thick PVN shocked between 7 and 18 GPa and (B) 700 nm PVN films shocked to 18 GPa. Arrows show the time at which the shock has fully traversed the film and rarefaction begins.

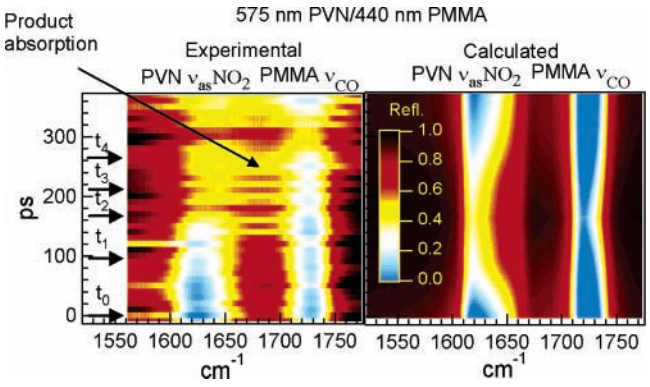

Figure 5. Time-resolved infrared absorption spectra (in reflectance units) of 575 nm PVN + 440 nm PMMA stacked films shocked to 18 GPa. The 1624 cm^{-1} peak is PVN $\nu_{as}(NO_2)$, and the 1728 cm^{-1} peak is PMMA's carbonyl stretch. Arrows denote timings: t_0, shock enters PVN; t_1, shock has fully transited PVN; t_2, shock has transited PMMA and rarefaction begins; t_3, head of the rarefaction fan reaches PVN/PMMA interface; t_4, head of the rarefaction fan reaches PVN/Al interface.

rarefaction is dispersive, the initial pressure drop at the head of the rarefaction fan is at the time denoted by the arrow. Only half of the loss of PVN absorption occurs by 100 ps; the rest of the absorption loss occurs while the shock is traversing the PMMA. There is a larger increase in absorption at times >130 ps, spread over higher frequencies, labeled "Product absorption" on Figure 5, than was apparent in the single PVN layer data. Again, there is no recovery of the initial PVN absorption loss after rarefaction. The PMMA absorption has also changed, which is likely caused by inaccurate accounting of thin film effects due to the significant refractive index changes in the reacted PVN, but at times >200 ps the PMMA may also be reacting. We do not yet know whether the decreased reflectivity at 300 ps is an experimental artifact or the rarefaction wave returning through the Al and reaching the Al/PVN interface.

It should be noted that both loss of reactant and gain of product absorptions may be occurring outside our range of spectral observation, and further experiments are required to more fully characterize the time-dependent shocked vibrational spectrum. Extension of the spectral ranges will also help identify possible products, and these initial experiments focused on the accessible spectral bandwidth around the nitro group stretches.

4. Discussion

The similar permanent loss of absorption in the $\nu_{as}(NO_2)$ and $\nu_s(NO_2)$ modes on shock loading indicates chemical reaction affecting the nitro group. The fact that the absorptions do not completely disappear may be due either to partial reaction quenched by the rarefaction or to formation of products that have absorptions in the same spectral regions; the latter possibility is suggested by Figure 5. Both nitrous acid (HONO),[30] a possible product from bimolecular reaction, and nitrogen dioxide (NO_2),[31] a possible product from unimolecular decomposition, are expected to have absorptions in both the $\nu_{as}(NO_2)$ and $\nu_s(NO_2)$ mode spectral regions. The spectra of such possible products are not yet known at these pressures and temperatures, and further experiments and calculations are required to quantitatively explain the reaction kinetics and identify the contributing reactions and products formed.

The observation that the reaction requires an induction time of tens of picoseconds, from the 18 GPa data of Figures 4B and 5, can aid in differentiating between proposed mechanisms of how the shock wave energy causes chemical reaction. An induction time of this magnitude is expected for reaction mechanisms that involve vibrational energy transfer, such as multiphonon up-pumping,[32] where the shock wave excites low-frequency phonons that multiply annihilate to excite the higher frequency modes. The induction time is also consistent with electronic excitation relaxing into highly excited vibrational states before dissociation,[33] and experiments are underway to search for electronic excitations. On the other hand, prompt mechanisms, such as direct high-frequency vibrational excitation by the shock wave, or direct electronic excitation[33] and prompt excited-state dissociation, should occur on subpicosecond time scales, in contrast to the data presented here.

5. Conclusions

At 17 and 18 GPa, poly(vinyl nitrate) films exhibited loss of absorption in the nitro group stretch modes that did not recover upon rarefaction, providing indication of initial chemical reaction. At pressures ≤9 GPa, the observed absorption loss recovered during the rarefaction as expected from thin film interference effects. At the higher pressures, loss of infrared absorption required an induction time of tens of picoseconds after shock passage, but did not require the rarefaction to release the pressure, as evidenced by shocking a PVN/PMMA double layer film. This induction time supports reaction mechanisms that require vibrational energy transfer rather than prompt reaction, but has not decisively identified the reaction mechanism. The infrared absorption results presented here demonstrate that it is possible to spectroscopically monitor shock induced

chemical reactions on picosecond time scales. This demonstration opens the door to further probing of such events with the myriad of ultrafast laser based spectroscopic tools now available, promising to provide more insight into the effects of extreme pressure and temperature jumps at the molecular scale.

Acknowledgment. The authors thank Darren Naud for PVN synthesis, Michael Oldenburg for the refractive index measurement of bulk PVN, Jose Archuleta for the density measurement of bulk PVN, Joe Tiee and Roger Petrin for loan of the infrared camera that made the experiments feasible, and our many colleagues who helped in early revision of the paper. This work was performed at Los Alamos National Laboratory under Department of Energy Contract No. W-7405-ENG.

References and Notes

(1) Moore, D. S.; Schmidt S. C. *J. Mol. Struct.* **1995**, *347*, 101.
(2) Schmidt, S. C.; Moore, D. S. *Acc. Chem. Res.*, **1992**, *25*, 427.
(3) Schmidt, S. C.; Schiferl, D.; Zinn, A. S.; Ragan, D. D.; Moore, D. S. *J. Appl. Phys.* **1991**, *69*, 2793.
(4) Dlott, D. D. *Acc. Chem. Res.* **2000**, *33*, 37.
(5) Dlott, D. D.; Hambir, S.; Franken, J. *J. Phys. Chem. B* **1998**, *102*, 2121.
(6) Hambir, S. A.; Franken, J.; Hare, D. E.; Chronister, E. L.; Baer, B. J.; Dlott, D. D. *J. Appl. Phys.* **1997**, *81*, 2157.
(7) Dreger, Z. A.; Gruzdkov, Y. A.; Gupta, Y. M.; Dick, J. J. *J. Phys. Chem. B* **2002**, *106*, 247.
(8) Engelke, R.; Pettit, D. R.; Sheffield, S. A. *J. Phys. Chem. A* **1997**, *101*, 1696.
(9) Renlund, A. M.; Sheffield, S. A.; Trott, W. M. *Shock Waves in Condensed Matter*; Gupta, Y. M., Ed.; Plenum: New York, 1986; pp 237−42.
(10) Trott, W. M.; Renlund, A. M. *Appl. Opt.* **24**, **1985**, *10*, 1520.
(11) Fickett, W.; Davis, W. C. *Detonation: Theory and Experiment*; Dover: New York, 2000.
(12) Reviews of shock wave research can be found in: *Shock Compression of Condensed Matter*; AIP: Melville, NY, biannually 1987−2001; and *First* through *Twelfth Symposium (International) on Detonation*; Office of Naval Research: Washington, DC, 1951−2002.
(13) Holian, B. L.; Germann, T. C.; Lomdahl, P. S.; Hammerberg, J. E.; Ravelo, R. *Shock Compression of Condensed Matter—1999*; Furnish, M. D., Chhabildas, L. C., Hixson, R. S., Eds.; AIP: Melville, NY, 2000; pp 35−43.
(14) Kadau, K.; Germann, T. C.; Lomdahl, P. S.; Holian, B. L. *Science* **2002**, *296*, 1681.
(15) Holian, B. L.; Lomdahl, P. S. *Science* **1998**, *280*, 2085.
(16) Strachan, A.; van Duin, C. T.; Chakraborty, D.; Dasgupta, S.; Goddard, W. A. *Phys. Rev. Lett.* **2003**, *91*, 98301/1-4.
(17) Kress, J. D.; Bickham, S. R.; Collins, L. A.; Holian, B. L.; Goedecker, S. *Phys. Rev. Lett.* **1999**, *83*, 3896.
(18) Brenner, D. W.; Robertson, D. H.; Elert, M. L.; White, C. T. *Phys. Rev. Lett.* **1993**, *70*, 2174.
(19) McGrane, S. D.; Moore, D. S.; Funk, D. J.; Rabie, R. L. *Appl. Phys. Lett.* **2002**, *80*, 3919−3921.
(20) Gahagan, K. T.; Moore, D. S.; Funk, D. J.; Reho, J. H.; Rabie, R. L. *J. Appl. Phys.* **2002**, *92*, 3679.
(21) McGrane, S. D.; Moore, D. S.; Funk, D. J. *J. Appl. Phys.* **2003**, *93*, 5063.
(22) McGrane, S. D.; Moore, D. S.; Funk, D. J. *Shock Compression of Condensed Matter*; 2003 AIP Proceedings, Portland, OR, July 20−25, 2003; American Institute of Physics: Melville, NY, 2004; p 1181. See ref 25.
(23) Funk, D. J.; Moore, D. S.; Gahagan, K. T.; Buelow, S. J.; Reho, J. H.; Fisher, G. L.; Rabie, R. L. *Phys. Rev. B* **2001**, *64*, 115114.
(24) Funk, D. J.; Moore, D. S.; McGrane, S. D.; Gahagan, K. T.; Reho, J. H.; Buelow, S. J.; Nicholson, J.; Fisher, G. L.; Rabie, R. L. *Thin Solid Films* **2004**, *542*, 453−454.
(25) Previously,[22] we were using a literature density value for PVN of $\rho = 1.6$ g/cm^3, while gas pychnometry of the material used provided a density of $\rho = 1.34$ g/cm^3, likely due to chain lengths different from the material density reported in ref 26. The pressures are determined by the equation $P = u_s u_p \rho_0$, where u_s and u_p were measured with dynamic ellipsometry, but the unshocked density ρ_0 was not directly measured in ref 22.
(26) Diepold, W. *Explosivstoffen* **1970**, *1*, 2.
(27) Moore, D. S.; McGrane, S. D.; Funk, D. J. *Appl. Spectrosc.* **2004**, *58*, 491.
(28) Gathers, G. R. *Selected Topics in Shock Wave Physics and Equation of State Modeling*; World Scientific Publishing: River Edge, NJ; 1994.
(29) Moore, D. S.; McGrane, S. D. *J. Mol. Struct.* **2003**, *661*, 561.
(30) Krajewska, M.; Olbert-Majkut, A.; Mielke, Z. *Phys. Chem. Chem. Phys.* **2002**, *4*, 4305.
(31) Sadtler Research Laboratories. *The Sadtler Handbook of Infrared Spectra*; Sadtler Research Laboratory: Philadelphia, 1978.
(32) Dlott, D. D.; Fayer, M. D. *J. Chem. Phys.* **1990**, *92*, 3798.
(33) Kuklja, M. M. *Appl. Phys. A* **2003**, *76*, 359.